Adsorption of Cyclohexane onto Activated Nanoporous Graphene: Modeling Using Artificial Neural Network

Zafari, Tahereh; Keyvani, Bahram; Mousavi, Mohsen
Department of Chemical Engineering, Saveh Islamic Azad University, I.R. IRAN

Rashidi, Alimorad*+
Nanotechnology Research Center, Research Institute of Petroleum Industry, Tehran, I.R. IRAN

ABSTRACT: *Industries pollute the environment by emitting organic substances known as Volatile Organic Compounds (VOC). One of the outstanding materials utilized to eliminate VOCs is nanoporous graphene. However, graphene's physical and chemical characteristics are influenced by a range of factors, including activation temperature, mass ratio, activation duration, adsorption capacity, N_2 adsorption-desorption, and morphology, Among other factors, the porosity of graphene is one of the crucial which has a direct influence on the adsorption capacity. In the current study, the adsorption capacity of graphene was investigated using cyclohexane and n-hexane adsorbents. In addition, the neural network has been employed to predict the adsorption capacity of graphene, and the Levenberg–Marquardt backpropagation (LM-BP) mechanism was utilized to determine model accuracy. The results show that at an activation temperature of 700°C, and mass ratio of 6, cyclohexane displayed a better performance with an adsorption capacity of 500 mg/g, as a comparison to n-hexane. The model demonstrated a suitable prediction with a correlation coefficient of 0.99966 (R^2) within the range of cyclohexane parameters such as impregnation ratio, activation time, and activation temperature between 3 to 9, 120 to 180 min, and 500 to 700°C respectively.*

KEYWORDS: *Adsorption; Artificial Neural Network (ANN); Chemical vapor deposition; Cyclohexane; n-hexane; Nanoporous graphene.*

INTRODUCTION

Nowadays, industrialization is considered a source of environmental contaminants [1]. Aromatics, ketones, esters, and aliphatic are the most important pollutants that are categorized as Volatile Organic Compounds (VOCs) [2]. Besides, contamination could cause diseases such as nervous syndromes [3]. The emission of these toxic pollutants into the air makes a great concern [4]. There are plenty of methods that were used to diminish the release of VOCs, such as adsorption[5], catalytic oxidation [6], condensation [7], and membrane separation [8]. Among them, adsorption is a cheap and significant method that plays a significant role in the separation process [9].

* *To whom correspondence should be addressed.*
+ *E-mail: rashidiam@ripi.ir*
1021-9986/2023/3/772-785 14/$/6.04

The adsorbents are categorized into two groups; first, adsorbents such as activated carbon (AC [10]), silica gel [11], activated alumina, and zeolites[12], second, Metal-Organic Frameworks (MOFs) [13]. However, the first group has a low cost, but VOCs have a low absorption capacity, and it has limitations during the process. On the other hand, adsorbent's type is one of the crucial factors in the process of adsorption, in which for the removal of VOCs there are plenty of adsorbents that have been studied as Activated Carbons (ACs), and most of them are acceptable due to large specific surface areas, low prices and environmental compatibility [14]. Although coal and asphaltum are considered a pioneer of AC, they have high costs. Graphene was first time discovered by *Novoselov et al* in 2004 [15]. However, due to the amazing properties of graphene, the desire to use graphene is high. A graphene molecular structure is a flat plate with hexagons consisting of carbon atoms [15]. It is one of the main allotropes of carbon and graphite materials are exposed in different dimensions [16]. Graphene has a two-dimensional structure based on graphitic forms of carbon, containing nothing-dimensional fullerenes and one-dimensional carbon nanotubes [17]. In addition, graphene has become an individual material because of its outstanding properties in electrical conduction, thermal conduction, high bulk density, portability of its load transports, optical conduction [18], and mechanical properties [19]. Currently, a significant difference of methods is used to make graphene. The most popular are mechanical peeling, chemical peeling, chemical synthesis, and Chemical Vapor Deposition (CVD) [20]. Recently, many types of research disclosed that graphene could be a suitable adsorbent for the VOCs removal [21]. Therefore, in the last decade, activated graphene that is used to remove various environmental pollutants has received special attention from researchers. However, demands for modeling of absorption processes due to a high conventional mathematical model are complex and challenging. Hence, the importance of artificial neural networks became highlighted to define nonlinear relationships between input and output data [22]. On the other hand, the effect of the porosity and external chemistry of the adsorbent in the VOC adsorption capacity has been investigated, and it has shown that both parameters were crucial [23].

In this research work for uptaking n-hexane and cyclohexane vapor, we developed and utilized a new sorbent based on carbon structure, which possesses excellent textural features that may significantly promote uptake capacity. The adsorption capacity has been predicted using an artificial neural network and experimental data has been used to evaluate the model's accuracy.

EXPERIMENTAL SECTION

Method & Materials

Materials

Comphor (Merck millipore), ZnO catalyst, Cyclohexane, n-Hexane, Hydrogen Chloride (18% w/w), Zinc Chloride ($ZnCl_2$), deionized (DI) water are used as a substrate material to study of removal of cyclohexane and n-hexane by adsorption process using activated nanoporous graphene.

Preparation of nanoporous graphene

To synthesize of nanoporous graphene, zinc oxide was deposited in a CVD reactor. The reactor has a 300 mm length and 50 mm diameter. The hydrogen gas enters to the reactor with a flow rate of 200 cc/min and reached 900°C within one hour; then the camphor carbon source was placed at a temperature of 900°C and the reaction is allowed to take place for 2-50 min. The remaining material consisting of 18% w/w hydrochloric acid was heated at 40°C for 5 hours. Finally, it was rinsed with deionized water and dried in an oven at a temperature of 90°C for 24 hours.

Activation of nanoporous graphene with $ZnCl_2$

In the current study, nanoporous graphene was activated with ratios of 3, 6, and 9 with $ZnCl_2$ as an activating agent in a furnace at a temperature of 500-700°C with a residence time of 2-3 h and rate of heating of 5°C/min using nitrogen gas. The activated graphene has been washed by 18% w/w hydrochloric acid at ambient temperature for 24 hours and then washed again with distilled water to neutralize the material, and finally dried in an oven at the temperature of 100°C for 24 hours.

Preparation method N-doped nanoporous graphene

N-doped nanoporous graphene has been obtained from melamine as a nitrogen source with a ratio of 1:1 in the furnace at a temperature of 700°C and heating rate of 5°C/min under nitrogen gas (flow rate of 100 cm^3/min)

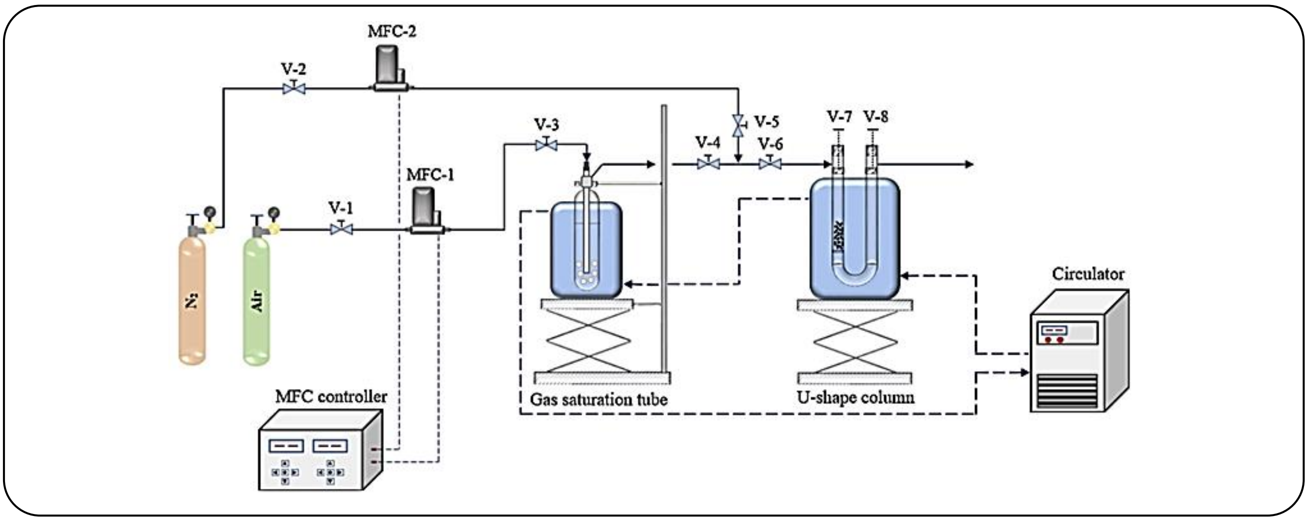

Fig. 1: The schematic of the VOC adsorption system [24].

with a residence time of 1 h. The sample was labeled NPG700.

VOCs vapor adsorption evaluation

The schematic of the experimental setup was used to measure the adsorption capacity of VOC vapor on activated graphene as an adsorbent at a temperature of 25°C and ambient pressure is shown in Fig 1. A mass flow controller (MFC-1) was used during the adsorption process to supply 130 cc/min of dry air as a carrier gas. The airflow from MFC-1 enters a glass bubbler containing VOC to produce saturated gas with VOC. The VOC-saturated air flows out of the bubbler and into the U-shaped tube containing the adsorbent. A water circulator was used to regulate the temperature of the bubbler and the adsorption column. The U-shaped container containing adsorbent and saturated gas was measured every 10 min, and the weight was defined using equation 1. M_{t0} and M_{ti} represent the weight of the adsorbent container at t = 0 and t = i of the adsorption time intervals, respectively. Q_{ti} represents the adsorption capacity of the adsorbent.

$$Q_{ti} = \frac{M_{ti} - M_{t0}}{M_{adsorbent}} \qquad (1)$$

Characterization

The textural properties of activated nanoporous graphene were measured using a static volumetric system by physical N_2 adsorption-desorption at -196.15°C (ASAP 2020). The specific surface area (S_{BET}) was obtained using the N_2 adsorption isotherm using the Brunauer–Emmett–Teller (BET) equation. The external surface area (S_{ext}) was defined using the t-plot method. The microporous specific surface area (S_{mic}) was determined using the variation between S_{BET} and S_{ext}. The total pore volume (V_t) adsorb at the relative pressure of 0.99. The micropore volume (V_{mic}) was determined using a t-plot method, and the mesopore volume (V_{mes}) was defined through the variation between V_t and V_{mic} [1].The morphology structures of synthesized nanocarbons were investigated using field-emission scanning electron microscopy on the TE-SCAN Model MIRA3. The analysis of surface functional groups was performed using Fourier Transform InfraRed (FT-IR) spectroscopy (Thermo Nicolet AVATAR 360) over the scan threshold of 4000–400 cm^{-1}.

RESULTS AND DISCUSSION

Investigation of the effect of a series of factors on the physical properties of activated graphene

Fig. 2 illustrates the N_2 adsorption and desorption isotherms and pore size distribution on the textural properties of activated nanoporous graphene. Table 1 shows the surface areas (S_{BET}, S_{mic}, S_{ext}) and pore volumes (V_t, V_{mic}, V_{mes}) of activated nanoporous graphene. Finally, Fig. 3 displays the association of preparation conditions and textural properties activated graphene (S_{BET} , S_{mic} , S_{ext}) and (V_t ,V_{mic} , V_{mes}).

Table 1: Physical properties of adsorption capacity cyclohexane of activated graphene.

Sample	Specific surface (m^2/g)			Pore volume (cm^3/g)			Capacity adsorption (mg/g)
	S_{BET}	S_{mix}	S_{ext}	V_t	V_{mix}	V_{mes}	
PG.9.500	100	48.7	52.50	0.49	0.015	0.4	263
PG.3.600	139	52.20	86.70	0.66	0.018	0.64	375
PG.6.700	130	55.43	74.34	0.57	0.019	0.55	500

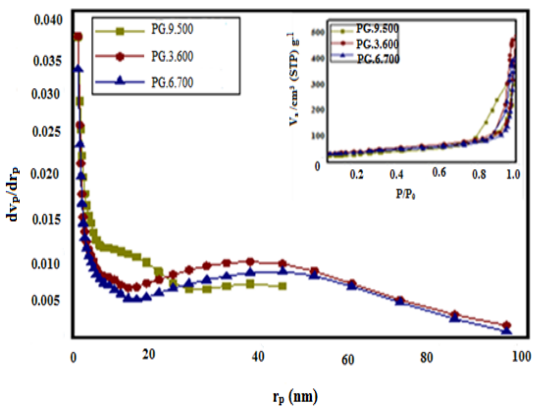

Fig. 2: N_2 adsorption-desorption isotherms of activated porous graphene.

Activation temperature

N_2 adsorption and desorption isotherms and pore size distribution of activated graphene at temperatures of 500°C, 600°C and 700°C with saturation ratios of 9, 3, and 6 and residence time of 2 and 3 hours are shown in Fig. 2. There is little distinction between all isotherms; at a relative pressure of 0.4, the adsorption isotherms correspond to the first category with a hysteresis ring, demonstrating the existence of micropores [25].Once the activation temperature grew from 500°C to 600°C, S_{BET} increased from 100 m^2/g to 139 m^2/g, and total pore volume has increased from 0.49 cm^3/g to 0.66 cm^3/g. Moreover, when activation temperature increases from 600°C to 700°C, the surface area and total pore volume decrease from 139 m^2/g to 130 m^2/g and from 0.66 cm^3/g to 0.57 cm^3/g, respectively. Also, the process became reduced when the activation temperature is further increased (> 700°C), the S_{BET}, and V_t mitigate due to the disorder of micropores [26].

Activation agent ratio ($ZnCl_2$)

According to Fig. 2, the N_2 adsorption-desorption isotherms and pore size distributions of nanoporous graphene were used for various $ZnCl_2$ ratios of 9, 3, and 6. The results show when the activation temperatures rise to 500°C, 600°C, 700°C, it was expected the activation time should be about 2-3 h. Moreover, when the activation agent ratio adjusts on 9, 3, and 6, the adsorption isotherm with hysteresis loop follows the type IV [27]. Hysteresis rings indicate that there are many mesopores in the adsorbents. Fig. 3(d) shows that by increasing an activation agent ratio, the ratio of mesopore volume in V_t was increased. Therefore, the proportion of microspores of V_t reduces. Furthermore, using an activation agent ratio of 3, 6, and 9 led to over berate the mesopores on graphene pores. In Fig. 3(c), the specific surface areas have similar behavior. These phenomena happen due to the expanding of pores and diffusion of volatile and the conversion of micropores to mesoporous in saturation ratios [28].

Activation time

Fig. 2 shows the N_2 adsorption-desorption isotherms and pore size distributions of graphene nanoporous that has been provided at various activation time between 2-3 hours. According to Fig. 2, all of the isotherms appears to be type IV, and the vast majority of the N_2 adsorption capacities are approximately the same due to all of the activation temperatures of 500°C, 600°C, and 700°C and the ratios of 9, 3, and 6. According to Fig. 3(e-f), the physical properties of activation graphene are proportionate with various activation times and similar to each other. It has been shown that the effect of activation time on their properties was significant compared to activation temperature and mass ratio. Furthermore, the activation time was more than 1 h, and within this period, the V_{mic} began to reduce, and the V_{mes} increased. This may be related to the pore magnitude that influences the lengthening of the activation time [28, 29].

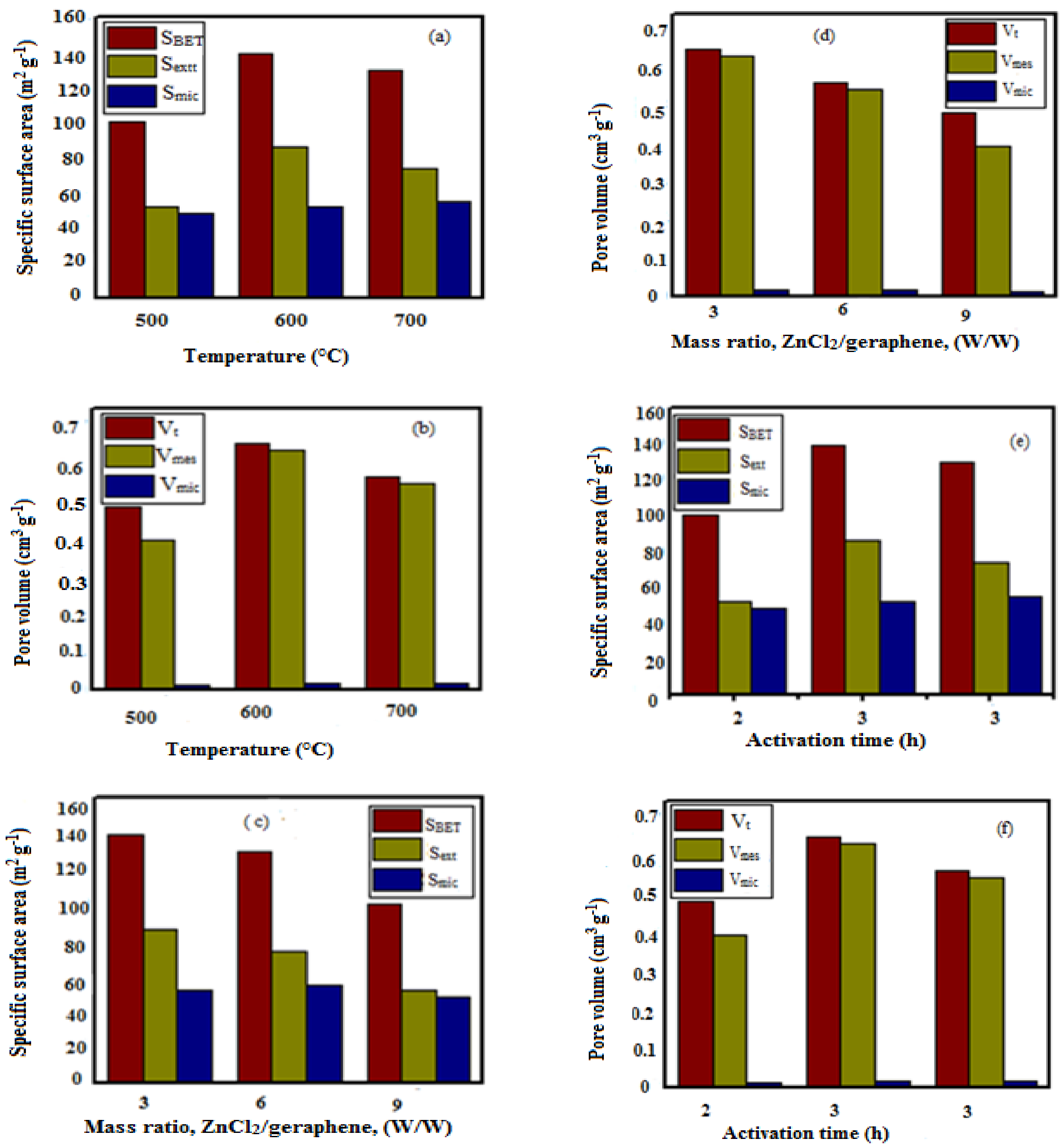

***Fig. 3:** Trends of preparation conditions and textural properties of the activated porous graphene (a-f).*

N_2 adsorption-desorption isotherms n-doped porous graphene

The N_2 adsorption-desorption isotherms of the nanoporous graphene and NPG700 templates were depicted in Fig. 4. The indicated isotherms display a typical curve of type IV based on the IUPAC. The hysteresis loop begins at the relative pressure of about 0.4 and displays mesopores graphene plates on edge [27]. In addition, the S_{BET}, the mean pore diameter, and total pore volume of the NPG700 and PG were highlighted in Table 2. Additionally, the porous graphene's physical properties were degraded due to the presence of the melamine precursor. Moreover, the existence of free nitrogen in the lattice graphene causes the graphene plates to absorb together, decreasing the surface area of the material [30].

Table 2: Physical properties of the n-doped porous graphene.

Sample	S_{BET} (m^2/g)	V_t (cm^3/g)	Mean pore diameter (nm)
PG	181.61	1.19	26.37
NG700	62.898	0.34	21.629

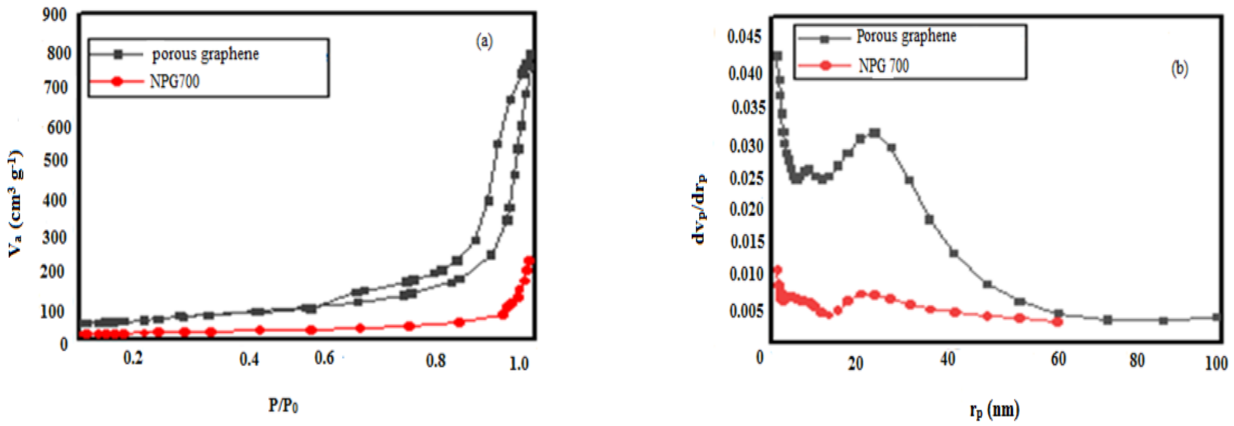

Fig. 4: N2 adsorption-desorption isotherms for n-doped porous graphene (a), Pore size distribution (b).

FT-IR analysis

The cyclohexane and n-hexane adsorption were determined by the changes of physical and chemical properties on the activated carbon surface [31]. The association of oxygen groups and aromatic ring electrons of cyclohexane and n-hexane was formed due to the interaction of both components. In this association, the oxygen atoms are electron-donors and aromatic rings are electron-acceptor [32]. The FT-IR spectra of porous graphene, PG.6.700+cyclohexane, and PG.6.600+n-hexane are indicated in Fig. 5. The FT-IR spectral positions and vibration bands interpretations are illustrated in Table 3. In addition, adsorption peaks are presented in Fig. 5. The spectrum indicates the intricate functional groups that exist in the sample. In the spectra of porous graphene, PG.6.700 and PG.6.600, the peaks appear at 3433.42 cm^{-1} and 3434 cm^{-1}, 3436 cm^{-1}, respectively. It can be related to the O-H stretching vibrations. The peaks at 2922, 1720.70, and 1633 cm^{-1} are related to C-H, C=O, and C=C stretching vibrations, respectively [33]. The band at 1384, 1406, and 1404 cm^{-1} are related to the C-O and phenols, respectively. Furthermore, the bands at 1104, 1108, and 1109 cm^{-1} are associated with the C-O stretching and band vibrations of C-OH, respectively [33]. FT-IR spectra of PG.6.700+cyclo and PG.6.600+hexane are compared with porous graphene. It represents several similar functional groups on the adsorbents. Moreover, the peaks of O-H stretching and C-O stretching vibrations are visible at 1104, 1086.87, and 1109 cm^{-1}, respectively. This indicates the performance of the oxygen functional group in the structure of organic materials. However, it seems the PG.6.700+cyclo shows more functional groups compared to PG.6.600+hexane. Therefore, it shows the higher adsorption capacity of cyclohexane on the higher adsorption capacity.

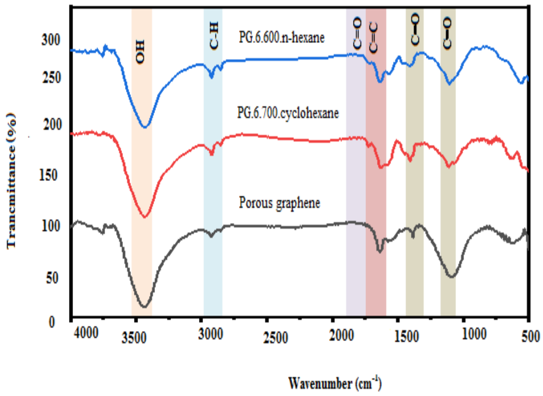

Fig. 5: FT-IR spectra of porous graphene and PG.6.700+cyclohexane, PG.6.600+n-hexane.

FE-SEM

The morphology of porous graphene is necessary before activation using $ZnCl_2$; therefore, to visualize the prerequisite porosity of the graphene, morphological

Table 3: Positions and the FT-IR spectral vibration bands.

Samples	Peak position in samples (cm^{-1})	Assignments	Peak position in reference	References
Porous graphene	3433.42	O-H stretching vibrations	3435	[34]
	2922.46	C-H stretching vibrations	2800	[33]
	1633.55	C=C stretching vibrations	1635	[35]
	1575.91	C=C stretching vibrations	1470	[35]
	1384.53	C-O stretching or C-O-C stretching	1270	[33]
	1086.87	C-O stretching and vibration in C-OH	1120	[33]
PG.6.700.cyclohexane	3434.03	O-H stretching vibrations	3433	[34]
	2922.34	C-H stretching vibrations	3000	[33]
	1720.70	C=O stretching vibrations	1720	[36]
	1633.50	C=C stretching vibrations	1620	[1]
	1406.05	C-O stretching	1249	[1]
	1109.34	C-O stretching and vibration in C-OH	1110	[37]
PG.6.600.hexane	3436.36	O-H stretching vibrations	3421	[1]
	2921.95	C-H stretching vibrations	2918	[1]
	1569.33	C=C stretching vibrations	1580	[37]
	1404.74	C-O stretching	1270	[33]
	1104. 73	C-O stretching and vibration in C-OH	1051	[1]

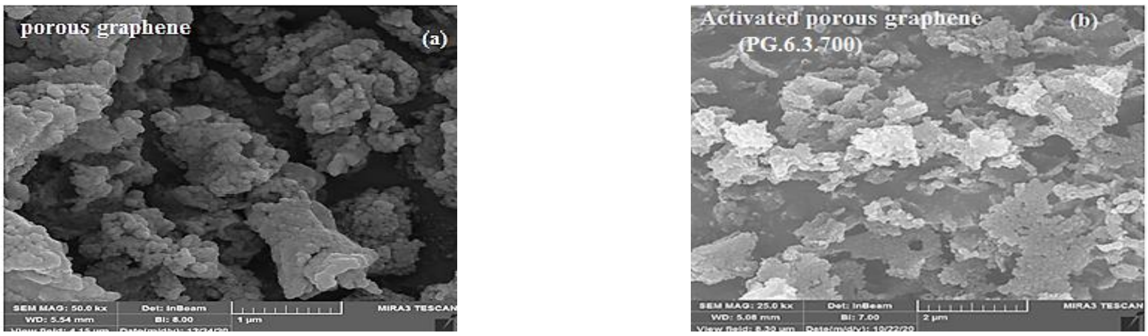

Fig. 6: FE-SEM images of the graphene before and after activation.

analysis were carried out using FESEM (Fig. 6a). FESEM images indicate the graphene planes crumpled together to create a disordered solid. The mean pore diameter (26.37 nm) can be observed in Fig. 6(b). High porosity was formed after the activation process, and this was demonstrated by the quantity of the adsorbed material.

Adsorption cyclohexane and n-hexane results

A gravimetric method was used to measure the adsorption capacity of cyclohexane and n-hexane vapors. The cyclohexane and n-hexane vapor adsorption was measured by allowing them to pass over the synthesized carbons through the U-shaped quartz glass using N_2 as a carrier gas. The process was carried out until a constant weight was obtained [37]Fig. 7 presents the adsorption capacity of cyclohexane and n-hexane vapor over activated carbons. The PG.6.3.700 has the highest efficiency with adsorbed amount of 500 mg/g for cyclohexane. Also adsorption capacity of PG.3.3.600 with a specific surface area of 139 m^2/g was 375 mg/g for cyclohexane. According to

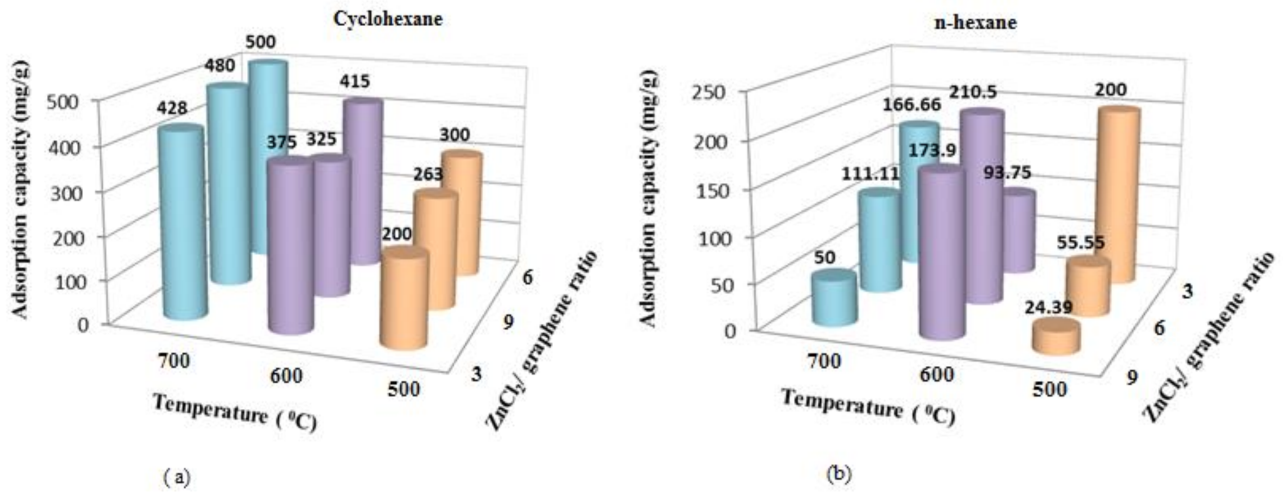

Fig. 7: Comparison of adsorption capacity for cyclohexane (a) and n-hexane (b) with different PGs.

the results, cyclohexane vapor adsorption capacities influenced other factors except for specific surfaces. PG.6.3.700 has micro/mesoporous structures. However, the presence of mesoporous increases the absorption capacity of the micropores that adsorbed cyclohexane vapor [37]. Table 1 shows that PG.3.3.600 has a better adsorption efficiency than others in terms of the pore volume. It can be observed that PG.3.3.600 has higher mesopore volumes, and it illustrates that mesopores play a significant role in cyclohexane adsorption. The existence of mesopores promotes dispersion in VOC molecules [1]. As a consequence, the absorption capacity increases as shown in Fig. 7 and Table 4. The results show different nanoporous graphene adsorption efficiency with a mass ratio of 3, 6, 9 and temperature of 500, 600, 700°C for n-hexane and cyclohexane on activated carbons. However, a comparison has been made between the adsorption capacity of cyclohexane and n-hexane. The results demonstrated that cyclohexane (500 mg/g) has a higher adsorption capacity than n-hexane with 210.5 mg/g. Table 5 represents the synthesized carbons' adsorption capacities compared to other materials. As observed, cyclohexane vapor adsorption capacities of PG.6.3.700 is outstanding with 500 mg/g. Consequently, a high-porosity of graphene was achieved using CVD that is activated with $ZnCl_2$.

Artificial Neural Network Function

The neural network with multilayer and post-propagation error-Lundberg-Marquardt (LM-BP) training algorithm was used to model the removal system [44, 45]. The temperature, duration, and saturation ratio were selected as input data, and cyclohexane removal was chosen as the target parameter (Fig. 8). In the model, the input data such as temperature, impregnation ratio, and time was entered in the excel sheet. Then the adsorption values of cyclohexane with nano sorbent are embedded on the same sheet as output data. After determining the input and output data, the data was divided into three parts: training data, validation, and testing [46, 47]. In the model, 70% of the data belongs to training, 15% belongs to validation, and 15% of the data were considered for tests. However, to reduce errors percentage and increase the accuracy of the estimated network weight and predicted values, the validation and testing of the network were repeated ten times for each stage of training. Fig. 9 represents the solidarity of the actual values and it was determined by the artificial neural network. The best line shows the best mean square error for the plotted network [48]. According to Fig. 10(a, b), correlation coefficient (R^2), mean of squared errors (mse), and the network training process are acceptable when the MSE value of the training curve hits the lowest point and test validated values get closer to each other. In step 4 of the training, the value is 3.3025 Fig. 9(b) shows that most of the available data is allocated in the training section and mostly placed around the baseline that indicates the correct prediction of the network. However, the percentage of allocated data to test and validation was suitable. Furthermore, in Fig. 11 the values are estimated using the neural network against

Table 4. Cyclohexane and n-hexane vapor adsorption results at 25°C on activated nanoporous graphene as an adsorbent.

Sample name	Factor 1	Factor 2	Factor 3	Response	
	Activation Temperature (°C)	Zinc Chloride/Graphene	Activation Time (min)	Experimental Cyclohexane Uptake (mg/g)	Experimental n-hexane Uptake (mg/g)
PG	500	3	120	200	200
PG	500	6	180	300	55.55
PG	500	9	120	263	24.39
PG	600	3	180	375	93.75
PG	600	6	120	415	210.5
PG	600	9	180	325	173.9
PG	700	3	120	428	166.66
PG	700	6	180	500	111.11
PG	700	9	120	480	50

Table 5: Adsorption capacities of the porous graphene compared with other samples.

Adsorbent	Adsorbate	Adsorption capacity (mg/g)	References
Activated carbon	Cyclohexane	330	[29]
Activated carbon	benzene	160	[38]
Durian shell activated	Toluene	57.14	[39]
Activated hydrocher	Cyclohexane	121.74	[40]
Activated carbon	Toluene	414.6	[1]
Activated GO/OMS	H_2(g)	23.4	[41]
Activated OMS	CH_4	33.6	[41]
Activated OMS	CO2	264	[41]
Activated OMS	H_2	21.6	[41]
Activated graphene	CO2	137.72	[42]
N-doped graphene composite	CO2	132	[43]
Activated PG.3.600	n-hexane	210.5	Current work
Activated PG.6.700	Cyclohexane	500	Current work
Activated PG.6.600	Cyclohexane	415	Current work

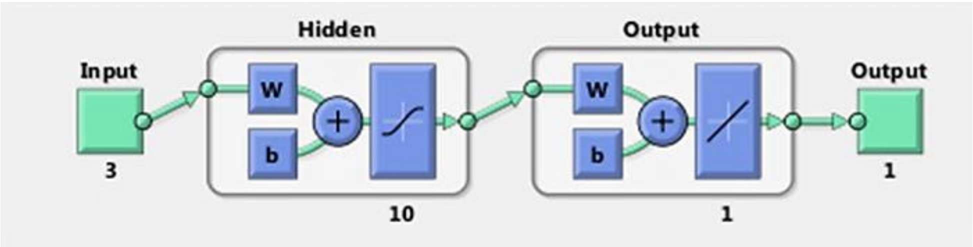

Fig. 8: Neural network function with inputs and outputs.

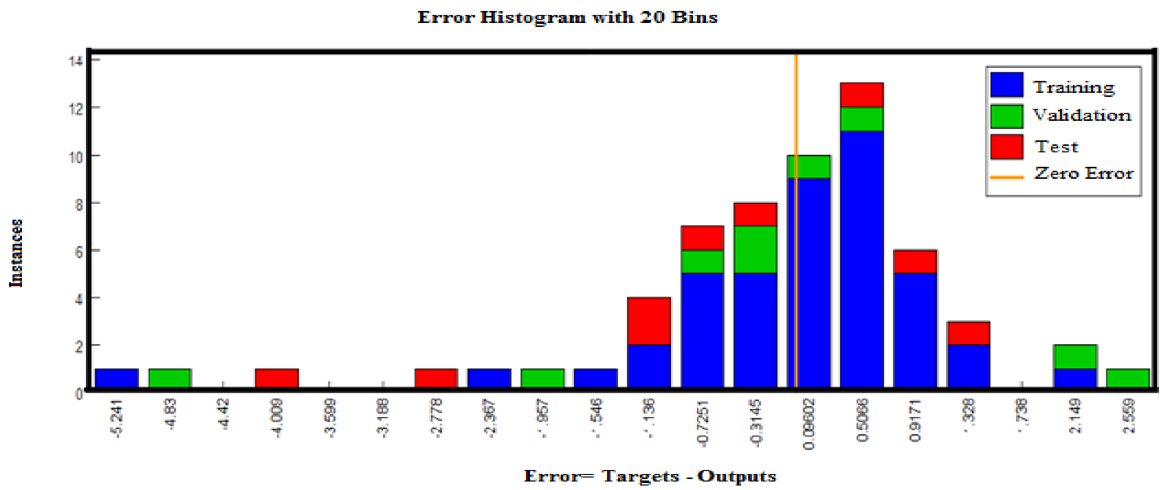

Fig. 9: Histogram of the obtained data for the selected network.

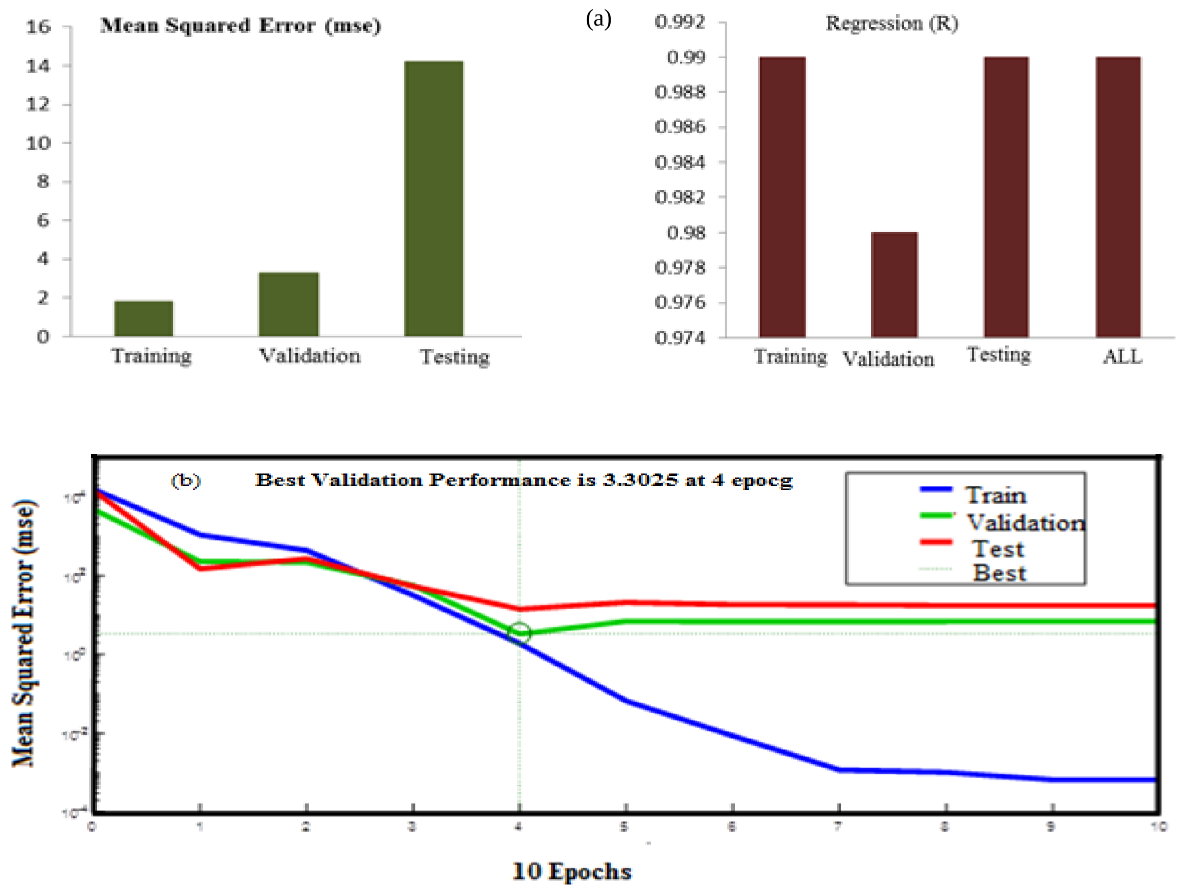

Fig. 10: The obtained values from the sum of the squares of error and the correlation coefficient of the selected neural network (a) and the sum of squares of error for the selected neural network (b).

the experimental values. The solidarity coefficient of the model is 0.99966 (R^2), which is an acceptable limit and entirely satisfactory [49].

CONCLUSIONS

A nanoporous graphene-based adsorbent was synthesized to eliminate cyclohexane and n-hexane vapors

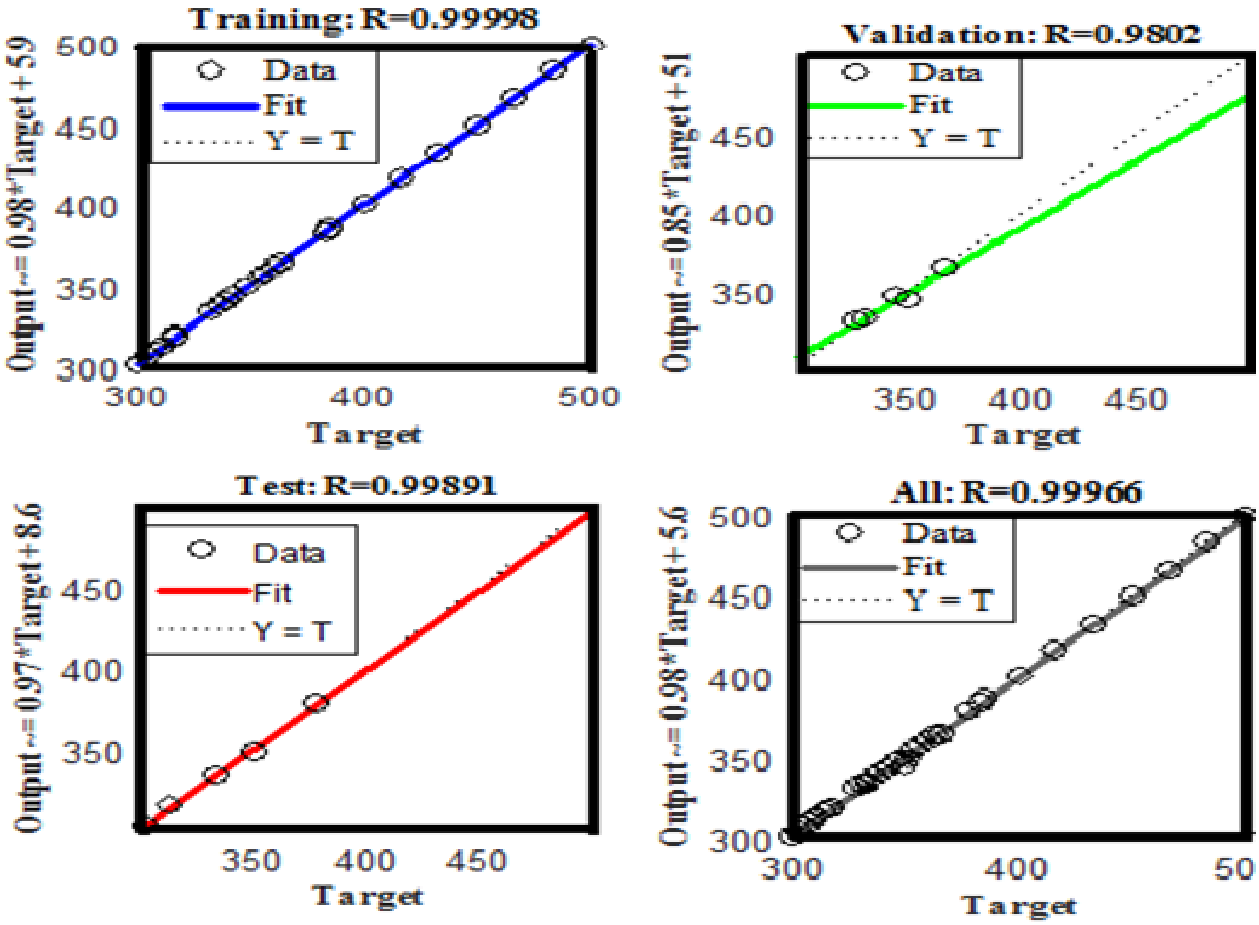

Fig. 11: Experimental values vs. predicted by neural network.

and the adsorption performance was evaluated. Moreover, the factors influencing the vapor uptake capacity, such as the ratio of objects, activation time, and reaction activation temperature, were also investigated. The Levenberg-Marquardt (LM-BP) artificial neural network model was employed to predict cyclohexane removal efficiency. According to the results, the n-hexane and cyclohexane uptake capacities were found to be 210.5 and 500 mg/g, respectively. Further, an increase in activation time, activation temperature, and saturation ratio of the reaction resulted in enhanced adsorption capacity for cyclohexane. The proposed neural network model displayed a good agreement with experimental results. Following the analysis of the model prediction precisions, the correlation for training data, test, and validation were also in good agreement with the experimental data.

Received :Mar. 20, 2022 ; Accepted : Jun. 13, 2022

REFERENCES

[1] Zhu J., Li Y., Xu L., Liu Z., Removal of Toluene From Waste Gas by Adsorption-Desorption Process Using Corncob-Based Activated Carbons as Adsorbents, *Ecotoxicology and Environmental Safety*, **165**: 115-125 (2018).

[2] Sui H., Liu H., An P., He L., Li X., Cong S., Application of Silica Gel in Removing High Concentrations Toluene Vapor by Adsorption and Desorption Process, *Journal of the Taiwan Institute of Chemical Engineers*, **74**: 218-224 (2017).

[3] Bernstein J.A., Alexis N., Bacchus H., Bernstein I.L., Fritz P., Horner E., *et al.*, The Health Effects of Nonindustrial Indoor Air Pollution, *Journal of Allergy and Clinical Immunology*, **121**: 585-591 (2008).

[4] Wang X., Ma C., Xiao J., Xia Q., Wu J., Li Z., Benzene/toluene/Water Vapor Adsorption and Selectivity of Novel C-PDA Adsorbents with High Uptakes of Benzene and Toluene, *Chemical Engineering Journal*, **335**: 970-978 (2018).

[5] Zhang S., Shao T., Kose H.S., Karanfil T., Adsorption of Aromatic Compounds by Carbonaceous Adsorbents: A Comparative Study on Granular Activated Carbon, Activated Carbon Fiber, and Carbon Nanotubes, *Environmental Science & Technology*, **44**: 6377-6383 (2010).

[6] Jiancai F., Xiao C., Qibin X., Hongxia X., Zhong L., Effect of Relative Humidity on Catalytic Combustion of Toluene over Copper Based Catalysts with Different Supports, *Chinese Journal of Chemical Engineering*, **17**: 767-772 (2009).

[7] Zaitan H., Bianchi D., Achak O., Chafik T., A Comparative Study of the Adsorption and Desorption of O-Xylene Onto Bentonite Clay and Alumina, *Journal of Hazardous Materials*, **153**: 852-859 (2008).

[8] Zhen H., Jang S.M., Teo W., Li K., Modified Silicone–PVDF Composite Hollow-Fiber Membrane Preparation and its Application in VOC Separation, *Journal of Applied Polymer Science*, **99**: 2497-2503 (2006).

[9] Tang L., Yu J., Pang Y., Zeng G., Deng Y., Wang J., *et al.*, Sustainable Efficient Adsorbent: Alkali-Acid Modified Magnetic Biochar Derived from Sewage Sludge for Aqueous Organic Contaminant Removal, *Chemical Engineering Journal*, **336**: 160-169 (2018).

[10] Zhang W., Cheng H., Niu Q., Fu M., Huang H., Ye D., Microbial Targeted Degradation Pretreatment: A Novel Approach to Preparation of Activated Carbon with Specific Hierarchical Porous Structures, High Surface Areas, and Satisfactory Toluene Adsorption Performance, *Environmental Science & Technology*, **53**: 7632-7640 (2019).

[11] Qin C., Guo H., Bai W., Huang J., Huang X., Dang X., *et al.*, Kinetics study on Non-Thermal Plasma Mineralization of Adsorbed Toluene over γ-Al2O3 Hybrid with Zeolite, *Journal of Hazardous Materials*, **369**: 430-438 (2019).

[12] Alivand M.S., Shafiei-Alavijeh M., Tehrani N.H.M.H., Ghasemy E., Rashidi A., Fakhraie S., Facile and High-Yield Synthesis of Improved MIL-101 (Cr) Metal-Organic Framework with Exceptional CO2 and H2S Uptake; the Impact of Excess Ligand-Cluster, *Microporous and Mesoporous Materials*, **279**: 153-164 (2019).

[13] Gil E.R., Ruiz B., Lozano M., Martín M., Fuente E., VOCs Removal by Adsorption onto Activated Carbons from Biocollagenic Wastes of Vegetable Tanning, *Chemical Engineering Journal*, **245**: 80-88 (2014).

[14] Cheli M., Fiori G., Iannaccone G., A Semianalytical Model of Bilayer-Graphene Field-Effect Transistor, *IEEE Transactions on Electron Devices*, **56**:2979-2986 (2009).

[15] Novoselov K.S., Geim A.K., Morozov S.V., Jiang D.-E., Zhang Y., Dubonos S.V., *et al.*, Electric Field Effect in Atomically Thin Carbon Films, *Science*, **306**: 666-669 (2004).

[16] Asgari R., Davoudi B., Polini M., Giuliani G.F., Tosi M., Vignale G., Quasiparticle Self-Energy and Many-Body Effective Mass Enhancement in a Two-Dimensional Electron Liquid, *Physical Review B*, **71**: 045323 (2005).

[17] Chen W., Yan L., Bangal P.R., Preparation of Graphene by the Rapid and Mild Thermal Reduction of Graphene Oxide Induced by Microwaves, *Carbon*, **48**: 1146-1152 (2010).

[18] Khan A.H., Ghosh S., Pradhan B., Dalui A., Shrestha L.K., Acharya S., *et al.*, Two-Dimensional (2D) Nanomaterials Towards Electrochemical Nanoarchitectonics in Energy-Related Applications, *Bulletin of the Chemical Society of Japan*, **90**: 627-648 (2017).

[19] Nair R.R., Blake P., Grigorenko A.N., Novoselov K.S., Booth T. J., Stauber T., *et al.*, Fine Structure Constant Defines Visual Transparency of Graphene, *Science*, **320**: 1308-1308 (2008).

[20] Geim A.K., Kim P., Carbon Wonderland, *Scientific American*, **298**: 90-97 (2008).

[21] Jiao L., Wang X., Diankov G., Wang H., Dai H., Facile Synthesis of High-Quality Graphene Nanoribbons, *Nature Nanotechnology*, **5**: 321-325 (2010).

[22] Hirani R.A.K., Asif A.H., Rafique N., Shi L., Zhang S., Wu H., *et al.*, Wastewater Remediation Technologies Using Macroscopic Graphene-Based Materials: A Perspective, *Frontiers in Nanotechnology*, **3**: 688552 (2021).

[23] Lillo-Ródenas M., Cazorla-Amorós D., Linares-Solano A., Behaviour of Activated Carbons with Different Pore Size Distributions and Surface Oxygen Groups for Benzene and Toluene Adsorption at Low Concentrations, *Carbon*, **43**: 1758-1767 (2005).

[24] Tehrani N.H.M.H., Alivand M.S., Rashidi A., Shamskar K.R., Samipoorgiri M., Esrafili M.D., *et al.*, Preparation and Characterization of a New Waste-Derived Mesoporous Carbon Structure for Ultrahigh Adsorption of Benzene and Toluene at Ambient Conditions, *Journal of Hazardous Materials*, **384**: 121317 (2020).

[25] Sui H., An P., Li X., Cong S., He L., Removal and Recovery of O-Xylene by Silica Gel Using Vacuum Swing Adsorption, *Chemical Engineering Journal*, **316**: 232-242 (2017).

[26] Lei B., Xie H., Chen S., Liu B., Zhou G., Control of Pore Structure and Surface Chemistry of Activated Carbon Derived from Waste Zanthoxylum Bungeanum Branches for Toluene Removal in Air, *Environmental Science and Pollution Research*, **27**: 27072-27092 (2020).

[27] Brunauer S., Deming L.S., Deming W.E., Teller E., On a Theory of the van Der Waals Adsorption of Gases, *Journal of the American Chemical Society*, **62**: 1723-1732 (1940).

[28] Yang J., Qiu K., Development of High Surface Area Mesoporous Activated Carbons from Herb Residues, *Chemical Engineering Journal*, **167**: 148-154 (2011).

[29] Popescu M., Joly J., Carre J., Danatoiu C., Dynamical Adsorption and Temperature-Programmed Desorption of VOCs (toluene, butyl Acetate and Butanol) on Activated Carbons, *Carbon*, **41**: 739-748 (2003).

[30] Hassani S.S., Samiee L., Ghasemy E., Rashidi A., Ganjali M.R., Tasharrofi S., Porous Nitrogen-Doped Graphene Prepared Through Pyrolysis of Ammonium Acetate as an Efficient ORR Nanocatalyst, *International Journal of Hydrogen Energy*, **43**: 15941-15951 (2018).

[31] Zhu M., Zhou K., Sun X., Zhao Z., Tong Z., Zhao Z., Hydrophobic N-Doped Porous Biocarbon from Dopamine for High Selective Adsorption of p-Xylene Under Humid Conditions, *Chemical Engineering Journal*, **317**: 660-672 (2017).

[32] Daifullah A., Girgis B., Impact of Surface Characteristics of Activated Carbon on Adsorption of BTEX, *Colloids and Surfaces A: Physicochemical and Engineering Aspects*, **214**: 181-193 (2003).

[33] Wang H., Sun Y., Zhu T., Wang W., Deng H., Adsorption of Acetaldehyde onto Carbide-Derived Carbon Modified by Oxidation, *Chemical Engineering Journal*, **273**: 580-587 (2015).

[34] Jang J., Miran W., Divine S.D., Nawaz M., Shahzad A., Woo S.H., *et al.*, Rice Straw-Based Biochar Beads for the Removal of Radioactive Strontium from Aqueous Solution, *Science of the Total Environment*, **615**: 698-707 (2018).

[35] Mohammed J., Nasri N.S., Zaini M.A.A., Hamza U.D., Ani F.N., Adsorption of Benzene and Toluene onto KOH Activated Coconut Shell Based Carbon Treated with NH3, *International Biodeterioration & Biodegradation*, **102**: 245-255 (2015).

[36] Kyzas G.Z., Lazaridis N.K., Deliyanni E.A., Oxidation Time Effect of Activated Carbons for Drug Adsorption, *Chemical Engineering Journal*, **234**: 491-499 (2013).

[37] Rahbar-Shamskar K., Azar P.A., Rashidi A., Baniyaghoob S., Yousefi M., Synthesis of Micro/Mesoporous Carbon Adsorbents by In-Situ Fast Pyrolysis of Reed for Recovering Gasoline Vapor, *Journal of Cleaner Production*, **259**:120832 (2020).

[38] Wibowo N., Setyadhi L., Wibowo D., Setiawan J., Ismadji S., Adsorption of Benzene and Toluene from Aqueous Solutions onto Activated Carbon and its Acid and Heat Treated Forms: Influence of Surface Chemistry on Adsorption, *Journal of Hazardous Materials*, **146**: 237-242 (2007).

[39] Tham Y., Latif P.A., Abdullah A., Shamala-Devi A., Taufiq-Yap Y., Performances of Toluene Removal by Activated Carbon Derived from Durian Shell, *Bioresource Technology*, **102**: 724-728 (2011).

[40] Zhang X., Xiang W., Wang B., Fang J., Zou W., He F., *et al.*, Adsorption of Acetone and Cyclohexane onto CO_2 Activated Hydrochars, *Chemosphere*, **245**: 125664 (2020).

[41] Szczęśniak B., Choma J., Jaroniec M., Effect of Graphene Oxide on the Adsorption Properties of Ordered Mesoporous Carbons Toward H_2, C_6H_6, CH_4 and CO_2, *Microporous and Mesoporous Materials*, **261**: 105-110 (2018).

[42] Tian Y., Lin Y., Hagio T., Hu Y.H., Surface-Microporous Graphene for CO_2 Adsorption, *Catalysis Today*, **356**: 514-518 (2020).

[43] Kemp K.C., Chandra V., Saleh M., Kim K.S., Reversible CO_2 adsorption by an Activated Nitrogen Doped Graphene/Polyaniline Material, *Nanotechnology*, **24**: 235703 (2013).

[44] Kavitha B., Sarala Thambavani D., Artificial Neural Network Optimization of Adsorption Parameters for Cr(VI), Ni(II) and Cu(II) Ions Removal from Aqueous Solutions by Riverbed Sand, *Iranian Journal of Chemistry and Chemical Engineering (IJCCE)*, **39**: 203-223 (2020).

[45] Mirshahvalad H., Ghasemiasl R., Raufi N., Malekzadeh Dirin M., A Neural Networks Model for Accurate Prediction of the Flash Point of Chemical Compounds, *Iranian Journal of Chemistry and Chemical Engineering (IJCCE)*, **39**: 297-304 (2020).

[46] Zahedi Abghari S., Imani A., Determination of Suitable Operating Conditions of Fluid Catalytic Cracking Process by Application of Artificial Neural Network and Firefly Algorithm, *Iranian Journal of Chemistry and Chemical Engineering (IJCCE)*, **37**: 157-168 (2018).

[47] Nasser M.R., Mohd A.H., Badrul M.J., Bawadia A., Online Composition Prediction of a Debutanizer Column Using Artificial Neural Network, *Iranian Journal of Chemistry and Chemical Engineering (IJCCE)*, **36(2)**: 153-174 (2017).

[48] Sadeghzadeh M., Maddah H., Ahmadi M.H., Khadang A., Ghazvini M., Mosavi A., *et al.*, Prediction of Thermo-Physical Properties of TiO_2-Al_2O_3/Water Nanoparticles by Using Artificial Neural Network, *Nanomaterials*, **10**: 697 (2020).

[49] Zolghadri A., Maddah H., Ahmadi M.H., Sharifpur M., Predicting parameters of Heat Transfer in a Shell and Tube Heat Exchanger Using Aluminum Oxide Nanofluid with Artificial Neural Network (ANN) and Self-Organizing Map (SOM)," *Sustainability*, **13**: 8824 (2021).